FCRAR 2020 - Proceedings

33rd Florida Conference on Recent Advances in Robotics

FCRAR 2020 - Proceedings

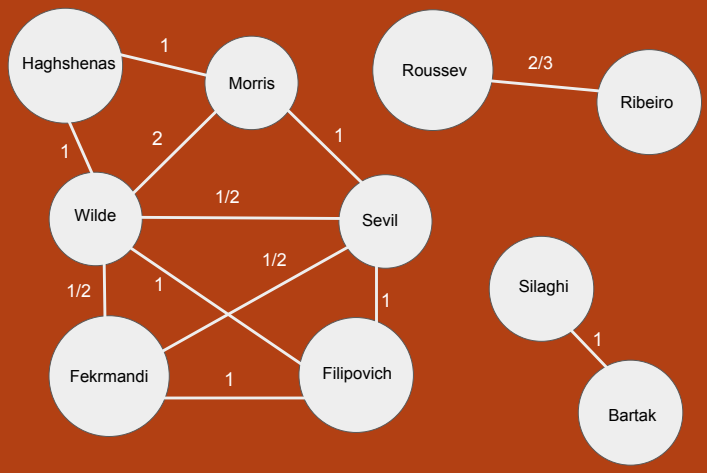

33rd Florida Conference on Recent Advances in Robotics

May 15th 2020

Florida Institute of Technology
High Tech with a Human Touch™

Edited by: M. C. Silaghi

Melbourne, Florida, USA
May 15th 2020

Cover by: Ioana Silaghi

PROCEEDINGS

Florida Conference on Recent Advances in Robotics (FCRAR)

Hosted by the

Florida Institute of Technology

May 15, 2020

Organizing Committee Members:

Marius Silaghi (chair)
Joerg Denzinger
Hadi Fekrmandi
Roman Filipovich
Hector Gutierrez
Ryan Integlia
Oren Masory
Melissa Morris
Julien Savaux
Hakki Erhan Sevil
Ryan Stansifer
Eskridge Thomas
Markus Wilde
Steven Wood

Robotics is an important research area at the intersection of most engineering fields and where recent advances impact on the whole society.

Copyright (c) is retained by the authors of each article.
Request permission to republish from each author separately.

Independent Publisher

Any remaining samples from this edition can be obtained from:
Marius C. Silaghi
Computer Engineering and Sciences Department
Florida Institute of Technology
150 West University Boulevard
Melbourne FL-32901
USA

Email: msilaghi@fit.edu

Anomaly Detection in the Joint Angle Sensors of a Snake Robot

Luke Fina[*], Hakki Erhan Sevil[†], and Mahdi Haghshenas-Jaryani[‡]

ABSTRACT

Anomaly detection method for joint angle sensors of a snake robot is introduced. The main goal of this study is to detect the joint sensor with anomaly using statistical approach along 3 joint angle sensors in a four-link snake type platform. In the developed approach, each joint sensor's measurement is taken into account and χ^2 hypothesis test is adopted, and orthogonal projection method is used for pin-pointing the sensor that has the anomaly. The presented study is applied to a snake robot model in a computer simulation environment. Results and discussions are provided, and according to simulation results, developed model successfully detects and isolates joint angle sensor with anomaly. This study is a part of larger effort toward developing resilient and intelligent robotic systems.
Keywords: Snake Robot, Anomaly Detection, Joint Control.

1. Introduction

Biologically inspired robots have become again an emerging field in robotics due to the demand for developing autonomous robotic systems with capability to adapt and operate in unknown and dynamic environments. Especially, biological snake has fascinated roboticists over the past five decades due to their versatile limbless locomotion mechanism which adapt easily to unstructured and unknown environments [1]. Ever since preliminary study of biological snake locomotion by Gray in 1946 [2] and development of the first snake robot by Hirose [3] in early 70's, enormous amount of work have been focused on developing dynamic models and control algorithms for modeling and controlling these complex robotic systems [4].

Most of snake robots studied over the past 45 years were considered as a kinematic chain with non-holonomic constraints that were explicitly imposed for avoiding lateral slip (sideslip constraints); a crucial factor for generating the serpentine locomotion of snake robots which is the most common locomotion gait between biological snakes [4]. However, these constraints are unrealistic in practice, as in the case of biological snakes, they rely on the interaction of their body with surrounding environment based on anisotropic friction properties to generate these motion constraints and consequently the progressive motion. In this work, these explicit non-holonomic constraints are eliminated in order to develop a more realistic dynamic model of snake robots while a robust joint control algorithm is developed to modulate the internal body motion of the snake robot to produce the required serpentine locomotion by attenuating lateral slip at each link. This control algorithm is implemented on a planar four-link snake robot with 6 degrees-of-freedom.

Considering snake type robotic platforms, there are not many examples in the literature in terms of anomaly and/or fault detection methods. In one study, a comparison between simulation model and real-life experiments based approach is introduced to detect actuator faults [5]. In a different study, a failure recovery system is presented for modular robotic platforms [6]. Although failure recovery is presented, the assumption is that the fault/failure information is available, thus detection part is not developed nor applied. Similarly, bio-inspired fault adaptive system design is presented in the literature, without providing details or suggestions on how to detect anomalies or faults [7]. In this study, our aim is to introduce a statistical based anomaly detection system applied to joint angle sensors of a snake robot. It is very crucial for a snake type platform to have a fault free sensor measurements in order to successfully control its motion. This study is our first step to accomplish robust robotic snake platforms.

The remainder of the paper is organized as follows. The next section describes the dynamical system model of the snake robot. The joint control of the snake robot and developed anomaly detection algorithm are described in Section 3 and Section 4, respectively. The Section 5 provides information about simulation design, results, and discussions. In the final section, conclusions and proposed future work are presented.

2. Dynamic System Model

Dynamics of a planar four-link snake robot as shown in Fig. 1 is described in this section. This is based on our earlier work [8, 9] where the dynamic model of a general n link snake robot was developed. In contrast to most common model of snake robots which consider a series of non-holonomic constraints apply to links of the robot in order to avoid lateral movement (side-slip condition), these constraints were eliminated in our model to represent more realistic model of snake robots. That leads to an under-actuated dynamic system where the internal shape motion is not anymore directly related to the overall displacement of the snake robot. The free body diagram of a link is shown in Fig. 2. The reaction forces, $\mathbf{F}_i$, $\mathbf{F}_{i+1}$ and torque at the proximal and distal joints associated with the link, τ_i^z, τ_{i+1}^z as well as the friction forces, F_i^n, F_i^t, and torque,τ_i^b, applied at the center-of-mass of the link are shown here. Friction force were modeled as Coulomb friction and the friction torque as a linear damping terms related to the angular velocity of the link. The equations of motion were derived using Kane's method as pre-

[*]Undergraduate student, Department of Mechanical Engineering, University of West Florida, Pensacola, FL 32514
[†]Assistant Professor, Department of Intelligent Systems & Robotics, University of West Florida, Pensacola, FL, 32514
[‡]Assistant Professor, Department of Mechanical & Aerospace Engineering, New Mexico State University, Las Cruces, NM, 88003

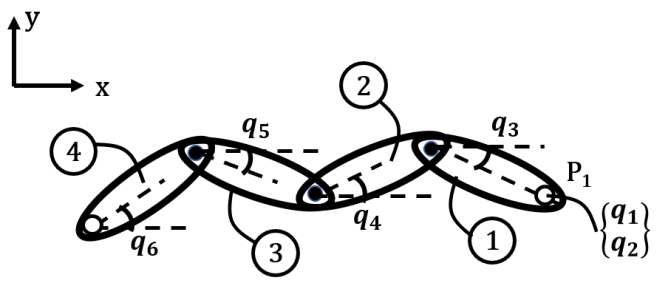

Figure 1. Overall Model of a Planar Snake Robot With Four Links and 3 Joints.

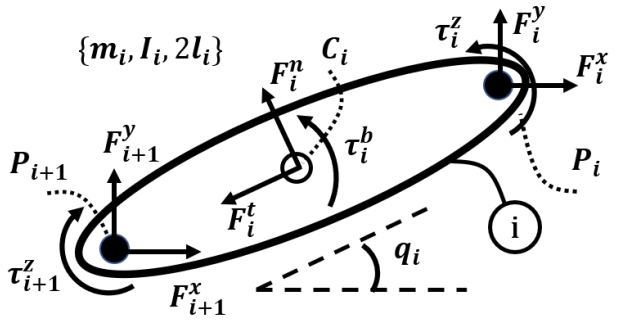

Figure 2. Free Body Diagram of a Snake Robot Link

sented in the general form of

$$M(\mathbf{q})\ddot{\mathbf{q}} + C(\mathbf{q},\dot{\mathbf{q}}) = J^T\mathbf{F} + B\tau \tag{1}$$

where the M is the symmetric and positive definite mass matrix, C is the nonlinear terms including centrifugal and Coriolis. External forces and moments acting on the snake robot (including friction forces and joint torques) are described by $\mathbf{F}$ and τ. $\mathbf{q} = [q_1, q_2, q_3, q_4, q_5, q_6]^T$ are the generalized coordinates describing the snake robot motion in 2D space where q_1 and q_2 are the coordinates of the tip of the snake robot (point P_1) and $[q_4, q_5, q_6, q_7]$ are the absolute rotational motion of the links with respect to the inertial frame O. $\dot{\mathbf{q}}$ and $\ddot{\mathbf{q}}$ are the first and second derivatives of the generalized coordinates, respectively. The equation of motion, Eq. (1), is derived using Kane's method where the differential equations are resultant of combination of two terms, the generalized inertial forces, F_r^*, and the generalized active forces, F_r, $r = \{1,\ldots,6\}$ where

$$\begin{aligned} F_r^* &= -\sum_{i=1}^{4}\left(m_i\mathbf{a}_i\cdot\mathbf{V}_i^r + [\mathbf{I}]_i\alpha_i\cdot\omega_i^r\right) \\ F_r &= \sum_{i=1}^{4}\left(\mathbf{F}_i\cdot\mathbf{V}_i^r + \tau_i\cdot\omega_i^r\right) \end{aligned} \tag{2}$$

$\mathbf{V}_i^r$ and ω_i^r are linear and angular partial velocities, respectively, defined as follows;

$$\begin{aligned} \mathbf{V}_i^r &= \frac{\partial\mathbf{V}_i}{\partial\dot{\mathbf{q}}_r} = \frac{\partial\mathbf{V}_{P_i}}{\partial\dot{\mathbf{q}}_r} + \frac{\partial\omega_i}{\partial\dot{\mathbf{q}}_r}\times\mathbf{r}_{P_iC_i} \\ &= \delta_{1,r}\hat{\mathbf{e}}_x + \delta_{2,r}\hat{\mathbf{e}}_y + \delta_{i+2,r}\hat{\mathbf{e}}_z\times\mathbf{r}_{P_iC_i} \end{aligned} \tag{3}$$

$$\omega_i^r = \frac{\partial\omega_i}{\partial\dot{\mathbf{q}}_r} = \delta_{i+2,r}\hat{\mathbf{e}}_z \tag{4}$$

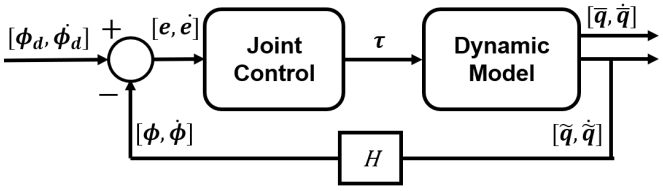

Figure 3. Joint Control Diagram.

where,

$$\delta i,j = \begin{cases} 1 & \text{if } i = j \\ 0 & \text{if } i \neq j \end{cases}$$

The active forces and moment acting on each body as shown in Fig. 2 are defined as

$$\begin{aligned} \mathbf{F}_i &= (F_i^x + F_{i+1}^x - \mu_n m_i g\ \mathrm{sgn}(V_i^n)\cos(q_i) - \\ &\quad \mu_t m_i g\ \mathrm{sgn}(V_i^t)\sin(q_i))\hat{\mathbf{e}}_x + \\ &\quad (F_i^y + F_{i+1}^y - \mu_n m_i g\ \mathrm{sgn}(V_i^n)\sin(q_i) - \\ &\quad \mu_t m_i g\ \mathrm{sgn}(V_i^t)\cos(q_i))\hat{\mathbf{e}}_y \\ \mathbf{M}_i &= \left(\tau_i^z + \tau_i^b - \tau_i^z\right)\hat{\mathbf{e}}_z \end{aligned} \tag{5}$$

and the inertial terms including linear and angular accelerations are defined as;

$$\begin{aligned} \mathbf{a}_i &= \ddot{q}_1\hat{\mathbf{e}}_x + \ddot{q}_2\hat{\mathbf{e}}_y + \alpha_i\times\mathbf{r}_{P_iC_i} + 2\omega_i\times\mathbf{V}_{P_i} \\ \alpha_i &= \ddot{q}_{i+2}\hat{\mathbf{e}}_z \end{aligned} \tag{6}$$

Substituting Eqs. (4, 5), and (6) back into Eq. (2) yields the equations of motion in Eq. (1). This set of equations will be used in the next section to derive the control algorithm in the joint space.

3. Joint Control of the Snake Robot

To generate the serpentine gait by the snake robot, the joints angle must be varying in a sinusoidal motion with amplitude α, phase shift of β, and bias γ as shown in Eq. (7)

$$\phi_i = \alpha\sin(\omega t + (i-1)\beta) + \gamma \tag{7}$$

To achieve this goal, a robust sliding mode controller is developed based on [8] for tracking control of joints of the snake-like robot in following the serpentine curve with parametric uncertainty as shown in Fig. 3. The forward dynamics of the snake robot provides the generalized coordinates and their derivatives after the numerical integration. The dynamic system's output, generalized coordinates, were split into the translational and rotational motion terms described by $\tilde{\mathbf{q}} = [q_1, q_2]$ and $\tilde{\mathbf{q}} = [q_3, q_4, q_5, q_6]$, respectively. The rotational part was used to determine the joint motion defined by the relative angles between two adjacent links as follows;

$$\phi = H\tilde{\mathbf{q}} \quad \text{and} \quad \dot{\phi} = H\tilde{\dot{\mathbf{q}}} \tag{8}$$

where,

$$H_{3\times4} = \begin{pmatrix} 1 & -1 & 0 & 0 \\ 0 & 1 & -1 & 0 \\ 0 & 0 & 1 & -1 \end{pmatrix}$$

Corresponding sliding mode manifold was defined based on the joint angle tracking error and its derivative

$$\mathbf{s} = \dot{\mathbf{e}} + \Lambda \mathbf{e} \tag{9}$$

where

$$\begin{aligned} \mathbf{e} &= \phi_d - \phi \\ \dot{\mathbf{e}} &= \dot{\phi}_d - \dot{\phi} \end{aligned} \tag{10}$$

The goal here is to design joint control action, τ, in order to the joint angles follow the desired sinusoidal trajectories presented in Eq. (7). Based on the sliding mode control approach, the control action is defined as

$$\tau = \tau_{eq} - K\text{sgn}(\mathbf{s}) \tag{11}$$

where τ_{eq} was determined by setting the time derivative of the sliding manifold in Eq. (9) equal zero and K is the diagonal matrix of control gains.

$$\dot{\mathbf{s}} = \ddot{\mathbf{e}} + \Lambda \dot{\mathbf{e}} = \mathbf{0} \tag{12}$$

Substituting from Eqs. (1) and (8) into Eq. (12), gives;

$$\begin{aligned} \tau_{eq} =& (H\tilde{M}^{-1}\hat{B})^{-1}\Big(\ddot{\phi}_d + \Lambda(\phi_d \\ & - H\dot{\tilde{\mathbf{q}}}) - H\tilde{M}^{-1}(-C + J^T F)\Big) \end{aligned} \tag{13}$$

To prove the stability of the closed loop control and determining the control gain matrix K, the following Lyapunov candidate function was selected

$$V = \frac{1}{2}\mathbf{s}^T\mathbf{s} \tag{14}$$

with following condition

$$\dot{V} \leq -\eta \mid \mathbf{s} \mid \tag{15}$$

where η is positive. Using Eq. (14), the $\dot{V}$ will be determined as follows,

$$\begin{aligned} \dot{V} = \mathbf{s}^T\dot{\mathbf{s}} = \mathbf{s}^T\Big(& \ddot{\phi}_d + \Lambda(\phi_d - H\dot{\tilde{\mathbf{q}}}) - \\ & H\tilde{M}^{-1}(-C + J^T F + B\tau)\Big) \end{aligned} \tag{16}$$

By substituting Eqs. (12) and (13) into Eq. (16) yields;

$$\begin{aligned} \mathbf{s}^T\Big(& -\Delta_B(\ddot{\phi}_d + \Lambda(\phi_d - H\dot{\tilde{\mathbf{q}}})) + \Delta_B H\tilde{M}^{-1}\hat{A} - \\ & H\tilde{M}^{-1}\Delta_A\Big) + K \mid \mathbf{s} \mid \leq -\eta \mid \mathbf{s} \mid \end{aligned} \tag{17}$$

where

$$\begin{aligned} A &= -C(\dot{\mathbf{q}}, \mathbf{q}) + J^T F \\ \Delta_A &= A - \hat{A} \\ \Delta_B &= B\hat{B}^{-1} - I_B \end{aligned}$$

Thus, by chosing the control gain matrix K as follows the condition in Eq. (15) will be satisfied.

$$\begin{aligned} K = (H\tilde{M}^{-1}B)^{-1}\Big[\eta I + \Big(& -\Delta_B(\ddot{\phi}_d + \Lambda(\phi_d - H\dot{\tilde{\mathbf{q}}})) + \\ & \Delta_B H\tilde{M}^{-1}\hat{A} - H\tilde{M}^{-1}\Delta_A\Big)\Big] \end{aligned} \tag{18}$$

4. Statistical Based Anomaly Detection

In this study, a statistical approach with chi-square test hypothesis is used for anomaly detection in the joint angle sensors of a snake robot[10, 11, 12, 13, 14]. The difference in measurement between different sensors is used to create residuals[15]. Three sensors at three joints of the snake robot are considered and the equations are provided correspondingly. The main assumption is that all three sensors have identical measurements with a phase shift, then the equation is written as

$$\begin{bmatrix} \phi_1(k) \\ \phi_2(k) \\ \phi_3(k) \end{bmatrix} = \begin{bmatrix} y(k) \\ y(k-k_1) \\ y(k-k_2) \end{bmatrix} + \begin{bmatrix} \xi_1(k) \\ \xi_2(k) \\ \xi_3(k) \end{bmatrix} + \begin{bmatrix} f_1(k) \\ f_2(k) \\ f_3(k) \end{bmatrix} \tag{19}$$

where $\phi_i(k)$ is the measured value from the i^{th} sensor of output state $y(k)$, $\xi_i(k)$ is the noise, and $f_i(k)$ is the fault value for the i^{th} sensor. The k_1 and k_2 are the phase shift values between sensor 1 and sensor 2, and between sensor 1 and sensor 3, respectively. The measurement noises $\xi_i(k), i = \{1,2,3\}$, are assumed to be normally distributed random sequences with zero mean and variance of σ^2 and independent from each other.

Equation (19) is pre-multiplied by the left null space of output state vector for eliminating the output state effect from the equation, then two-dimensional vector becomes

$$\mathrm{T}(k) = \mathbf{V}\mathrm{Y}(k) = \mathbf{V}\Xi(k) + \mathbf{V}\mathrm{F}(k) \tag{20}$$

where $\mathrm{T}(k) = [\tau_1(k)\ \tau_2(k)]^T \in \mathbb{R}^{2\times 1}$ is defined as the residuals, which are to indicate any anomaly in any sensor of the snake robot, $\phi_i(k), i = \{1,2,3\}$.

In the normal case, the expected values of the residuals have a zero mean, on the other hand, if there is an anomaly, the expected value will be a non-zero value. This observation is used to set the hypothesis test for detecting anomaly as

$$\begin{aligned} H_0 &: E[\bar{\mathrm{T}}(k)] = 0 \\ H_1 &: E[\bar{\mathrm{T}}(k)] \neq 0 \end{aligned} \tag{21}$$

where the acceptance of the hypothesis is carried out by the second degree chi-square test as

$$\chi^2(2,k) = \gamma(k) = \bar{\tau}_1^2(k) + \bar{\tau}_2^2(k) \tag{22}$$

The χ^2 random variable $\gamma(k)$ is compared to h, which is a threshold value, for detecting the anomaly.

$$\Pr(\gamma(k) \leq h) = 1 - \alpha \tag{23}$$

If $\gamma(k)$ is equal or smaller than the threshold value, that means the system is normal. Contrary to that, if it's greater than threshold value, there is an anomaly on a sensor, with a false alarm probability of α. Once anomaly is detected, the isolation is performed by checking orthogonal projection of the fault vector on the null space[16], using ϑ as

$$\vartheta_i(k) = \left\| \frac{\bar{\mathrm{T}}(k)}{\|\bar{\mathrm{T}}(k)\|} - \frac{\mu_i}{\|\mu_i\|} \right\|, \ i = \{1,2,3\} \tag{24}$$

where μ_i is the normalized i^{th} column vector of the null space. Among $\vartheta_1(k)$, $\vartheta_2(k)$ and $\vartheta_3(k)$, the smallest $\vartheta_i(k)$ is

$$\vartheta_l(k) = \min\{\vartheta_i(k), i = 1,2,3\} \tag{25}$$

which will indicate the l^{th} sensor as the faulty one because the residuals will be shifted in the direction of the l^{th} column of the null space matrix. It should also be noted that, in this study, it is assumed that only one sensor has anomaly at a given time.

5. Results of Simulations and Discussions

The simulation experiments are accomplished by using 3 joint angle sensors in simulation environment. During the simulation runs, the snake robot is commanded to navigate in a straight line. The anomaly detection sub-system is designed to be just for providing information on anomaly, i.e. it is passive. In this study, the anomaly detection system is not integrated into the feedback control system; it runs as a separate unit.

The simulation consists of 4-link snake robot dynamic model, and the joint controller. In the simulations, the variance of sensor noise for joint angle measurements is set as 0.002 $(rad)^2$ [17]. The simulation is run for 30 seconds. In the resulting plots, the time starts from 5 seconds in order to eliminate the effect of different movements of the joints at the beginning of the simulation. The anomaly detection is based on the main assumption of the sensors are fault-free and identical. There is phase shift between different joints, and time delays are introduced for the sensors as, 0.17 seconds between sensor 1 and sensor 2, 0.33 seconds between sensor 1 and sensor 3. In the first simulation run, there is no anomaly added to the sensors.

The joint angle measurements are depicted in Fig. 4. The anomaly alarm index and anomaly sensor index plots are given in Fig. 5. The alarm index value gives 0 when there is no anomaly detected, and gives 1 when anomaly is detected. The sensor index provides the isolation information of the sensor with anomaly. It should be noted both alarm and sensor index results have false positives with probability α, which is set to 1%.

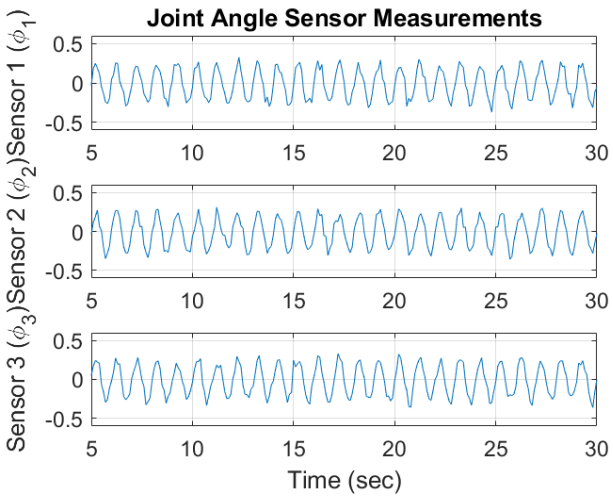

Figure 4. Joint Angle Measurements - No Fault Injected

As there is no anomaly existing in the sensors, orthogonal projection difference of the residuals scatter and they do not statistically favor any specific vector direction, meaning there is no anomaly detected. Moreover, alarm index and sensor index are presented

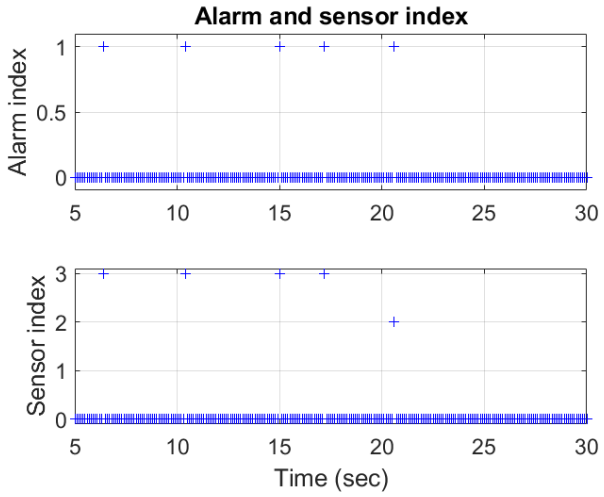

Figure 5. Alarm and Anomaly Index Values - No Fault Injected

in Fig. 5. The top plot shows the alarm index which equals to 1 whenever an anomaly is detected, and equals to zero otherwise. It can be seen that alarm index randomly gives value of 1 when there is no fault injected because of the false alarm probability, and total number of 1 values are less than 1%. The bottom plot in Fig. 5 depicts the sensor isolation index plot. The sensor index points out the sensor number that has the anomaly. Similarly, because of the false alarm probability, the sensor index gives 1, 2, or 3 in a random fashion even though no anomaly exists.

In the second simulation run, a fault is injected to the third sensor after 15 seconds in the simulation, for a duration of 10 seconds. The resulting sensor measurements are depicted in Fig. 6. Due to the injected anomaly, the third sensor has a biased type fault in its measurements. Furthermore, the anomaly values are given on Fig. 7.

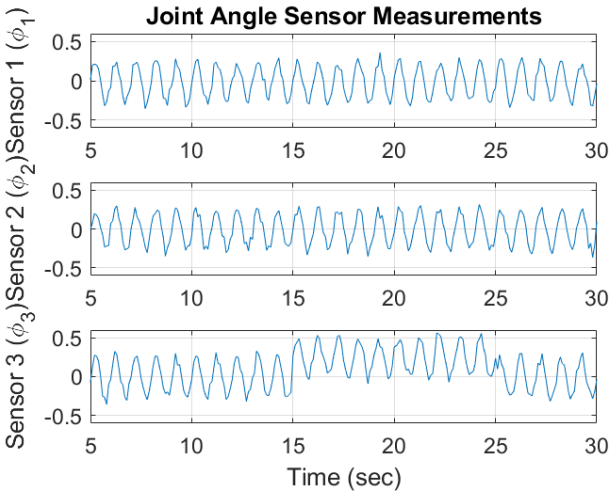

Figure 6. Joint Angle Measurements - Fault Injected

In the fault injected case, the developed method successfully detects the anomaly and pinpoints the sensor that has it (Fig. 7). In Fig. 7, alarm index and sensor index values are shown for joint angle measurements. During the anomaly occurrence from 15 to

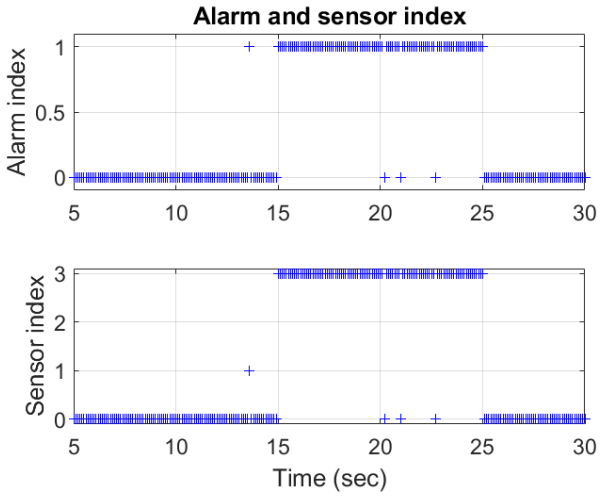

Figure 7. Alarm and Anomaly Index Values - Fault Injected

25 seconds of the simulation, the alarm index notifies the detection by giving value 1 consistently. Moreover, the sensor index marks sensor number 3 as the faulty sensor.

6. Conclusions

This paper introduces a anomaly detection method for joint angle sensors of a snake robot. For the detection part, the χ^2 hypothesis test is adopted, and isolation is performed by comparing orthogonal projections of three joint angle sensors. Simulation results are presented with successful implementation of the anomaly detection for an additive (bias) type fault in any of the three joint sensors. As future works, the developed system will be tested with different kind of faults, such as gain type, and parameter analysis will be added to determine robustness of the system considering noise levels and fault magnitudes. Furthermore, the effect of faulty sensor on the system dynamics will be discussed and robust fault tolerant controller design will be developed.

References

[1] K. Dowling, "Limbless locomotion: learning to crawl," in *Proceedings 1999 IEEE International Conference on Robotics and Automation (Cat. No. 99CH36288C)*, vol. 4, pp. 3001–3006, IEEE, 1999.

[2] J. Gray, "The mechanism of locomotion in snakes," *Journal of experimental biology*, vol. 23, no. 2, pp. 101–120, 1946.

[3] S. Hirose, *Biologically inspired robots: snake-like locomotors and manipulators*, vol. 1093. Oxford university press Oxford, 1993.

[4] P. Liljebäck, K. Y. Pettersen, . Stavdahl, and J. T. Gravdahl, "A review on modelling, implementation, and control of snake robots," *Robotics and Autonomous Systems*, vol. 60, pp. 29–40, Jan. 2012.

[5] V. Mehta, S. Brennan, and F. Gandhi, "Experimentally verified optimal serpentine gait and hyperredundancy of a rigid-link snake robot," *IEEE Transactions on Robotics*, vol. 24, no. 2, pp. 348–360, 2008.

[6] V. Vonásek, D. Oertel, S. Neumann, and H. Wörn, "Failure recovery for modular robot movements without reassembling modules," in *2015 10th International Workshop on Robot Motion and Control (RoMoCo)*, pp. 136–141, IEEE, 2015.

[7] M. Arroyo, N. Huisman, and D. C. Jensen, "Exploring natural strategies for bio-inspired fault adaptive systems design," *Journal of Mechanical Design*, vol. 140, no. 9, p. 091101, 2018.

[8] M. Haghshenas-Jaryani and G. Vossoughi, "Modeling and sliding mode control of a snake-like robot with holonomic constraints," in *2008 IEEE International Conference on Robotics and Biomimetics*, pp. 454–461, 2009.

[9] M. Haghshenas-Jaryani and G. Vossoughi, "Trajectory control of snake-like robots in operational space using a double layer sliding mode controller," in *ASME 2015 International Design Engineering Technical Conferences and Computers and Information in Engineering Conference*, pp. V05AT08A053–V05AT08A053, American Society of Mechanical Engineers, 2015.

[10] H. E. Sevil and A. Dogan, "False fault detection in airdata sensor due to nonuniform wind in aerial refueling," in *AIAA Atmospheric Flight Mechanics Conference*, p. 6446, 2011.

[11] H. E. Sevil, "Airdata sensor based position estimation and fault diagnosis in aerial refueling," phd dissertation, The University of Texas at Arlington, Arlington, TX, USA, 2013.

[12] H. E. Sevil and A. Dogan, "Airdata sensor fault detection and isolation for receiver aircraft in aerial refueling," in *Proc. of ASM 2013, AIAA Aerospace Sciences Meeting*, (Grapevine, USA), 7-10 January 2013. AIAA 2013-0950.

[13] H. E. Sevil and A. Dogan, "Fault diagnosis in air data sensors for receiver aircraft in aerial refueling," *AIAA Journal of Guidance, Control and Dynamics*, vol. 38, no. 10, pp. 1959–1975.

[14] H. E. Sevil, "Anomaly detection using parity space approach in team of UAVs with entropy based distributed behavior," in *Proc. of AIAA Scitech 2020 Forum*, (Orlando, USA), 6-10 January 2020. AIAA 2020-1625.

[15] I. Hwang, S. Kim, Y. Kim, and C. E. Seah, "A survey of fault detection, isolation, and reconfiguration methods," *IEEE transactions on control systems technology*, vol. 18, no. 3, pp. 636–653, 2010.

[16] P. M. Frank, "Fault diagnosis in dynamic systems using analytical and knowledge-based redundancy: A survey and some new results," *automatica*, vol. 26, no. 3, pp. 459–474, 1990.

[17] H. E. Sevil and A. Dogan, "Investigation of measurement noise effect on wind field estimation using multiple UAVs," in *Proc. of AIAA Scitech 2019 Forum*, (San Diego, USA), 7-11 January 2019. AIAA 2019-1601.